Energy & Environmental Science

Crosslinked Fluoropolymers Exhibiting Superior High-Temperature Energy Density and Charge-Discharge Efficiency

Journal:	*Energy & Environmental Science*
Manuscript ID	EE-ART-11-2019-003603.R2
Article Type:	Paper
Date Submitted by the Author:	03-Mar-2020
Complete List of Authors:	Li, He; The Pennsylvania State University, Materials Science and Engineering Gadinski, Matthew ; The Pennsylvania State University, Materials Science and Engineering Huang, Yuqi ; The Pennsylvania State University, Materials Science and Engineering Ren, Lulu; The Pennsylvania State University, Materials Science and Engineering Zhou, Yao; Pennsylvania State University University Park, Department of Materials Science and Engineering Ai, Ding; The Pennsylvania State University, Materials Science and Engineering Han, Zhubing; The Pennsylvania State University, Materials Science and Engineering Yao, Bin; The Pennsylvania State University, Materials Science and Engineering Wang, Qing; The Pennsylvania State University, Materials Science and Engineering

Journal Name

ARTICLE

Crosslinked Fluoropolymers Exhibiting Superior High-Temperature Energy Density and Charge-Discharge Efficiency

Received 00th January 20xx,
Accepted 00th January 20xx

DOI: 10.1039/x0xx00000x

www.rsc.org/

He Li, Matthew R. Gadinski, Yuqi Huang, Lulu Ren, Yao Zhou, Ding Ai, Zhubing Han, Bin Yao and Qing Wang*

The electrification of transport requires dielectric materials capable of operating efficiently at high temperatures to meet the increasing demand of electrical energy storage at extreme conditions. Current high-temperature dielectric polymers rely on the incorporation of wide bandgap inorganic fillers to restrain electrical conduction and achieve high efficiencies at elevated temperatures. Here, we report a new class of all-polymer based high-temperature dielectric materials prepared from crosslinking of melt-processable fluoropolymers. The crosslinked polymers exhibit larger discharged energy densities and greater charge-discharge efficiencies along with excellent breakdown strength and cyclic stability at elevated temperatures when compared to the current dielectric polymers. The origins of the marked improvement in the high-temperature capacitive performance are traced to efficient charge-trapping by a range of the molecular trapping centers resulted from the crosslinked structures. In addition, the implementation of melt-extrudable polymers would enable scalable processing that is compatible with the current fabrication techniques used for polymer dielectrics, which is in sharp contrast to the dielectric polymer composites with inorganic fillers.

1. Introduction

Although dielectric materials capable of operating at high temperatures is of increasing importance for advanced electronics and electric power systems, the control of charge carrier transport in organic materials at elevated temperatures is fundamentally challenging.[1,2] Polymers generally display the characteristics of thermally activated charge transport, leading to sharply increased leakage currents with increasing temperature.[3-5] Consequently, while polymer dielectrics are the preferred materials for energy storage capacitors owing to their high breakdown strength and low loss,[6–16] their performance typically optimized for operation at ambient temperature declines significantly with the increase of working temperatures.[17–20] For example, the discharge efficiency (η, $\eta = U_e/U_o \times 100\%$, U_e: discharged energy density, U_o: stored energy density) of biaxially oriented polypropylene (BOPP) films, which is the best commercially available dielectric polymer, decreases steeply from 96.2% to 87.4% and 68.5% with increasing temperature from 25 °C to 80 °C and 120 °C, respectively, at an applied field of 400 MV m^{-1}. On the other hand, the rapidly evolving electrification of transportation demands electric power systems to be located in or near engines possessing high temperatures.[19–21] For instance, polymer capacitors are essential components of power inverters in electric vehicles, where the working temperature is around 150 °C. Wide bandgap semiconductors, *e.g.* silicon carbide and gallium nitride, which offer opportunities to transform microelectronics, also require next-generation capacitors to sustain temperatures ≥150 °C.[2,22]

There are a variety of high-performance polymers, including polyimide (Kapton® PI), polycarbonate (PC), polyetherimide (PEI), poly(ether ketone) (PEEK) and fluorene polyester (FPE), which have been examined to replace BOPP for high-temperature capacitive applications in energy storage and power conditioning.[18–20] The primary strategy is the utilization of high glass transition (T_g) polymers to provide thermal and dielectric stability at elevated temperatures. Although stable weak-field dielectric properties have been revealed in these polymers up to their respective T_g, the polymers are unable to efficiently impede electrical conduction under elevated temperatures and high electric fields.[5,19,20] The thermally- and electrically-activated charges increases exponentially with temperature and applied field, giving rise to high conduction loss and a poor η.[23–25] For example, at 150 °C, the electrical conductivity (σ) of PI increases from 6.8×10^{-13} S m^{-1} at 50 MV m^{-1} to 3.5×10^{-11} S m^{-1} at 250 MV m^{-1}, resulting in a sharp reduction in η from 97.6% to 55.7%. More recently, improved high-temperature dielectric performance has been demonstrated in a class of dipolar glass polymers based on sulfonylated poly(2,6-dimethyl-1,4-phenylene oxide) (SO_2-PPO) and polymers of intrinsic microporosity (SO_2-PIM).[26,27] Until now, the introduction of wide bandgap inorganic materials such as boron nitride nanosheets (BNNSs) into polymers to form the polymer composites has been the most effective approach to controlling electrical conduction and achieving high η for elevated-temperature capacitive energy storage.[17,28]

Here we present all-polymer high-temperature capacitive materials based on the crosslinked polymers, which exhibit superior electric discharging performance to the current dielectric polymers at high temperatures. It is found that the crosslinked molecular

Department of Materials Science and Engineering, The Pennsylvania State University, University Park, Pennsylvania, 16802, USA.
E-mail: wang@matse.psu.edu
†Electronic Supplementary Information (ESI) available: Structural characterizations, more electrical property measurements. See DOI: 10.1039/x0xx00000x

structures efficiently function as deep traps to inhibit charge carrier transport in polymers at high temperatures and applied electric fields.

Note that the crosslinking of polyethylene (PE) is carried out industrially to improve impact and tensile strength, environmental stress crack resistance, creep and abrasion resistance of PE, which yields crosslinked polyethylene (XLPE) for electrical insulations.[29] Additionally, crosslinking has been shown to be a successful means of enhancing electrochemical stability of poly(ethylene oxide) (PEO)-based electrolytes,[30] and reducing ferroelectric hysteresis and improving polarization of ferroelectric polymers for improved U_e and η at ambient temperature.[31–34] Nevertheless, none of the early studies demonstrates the effectiveness of crosslinking in reducing conduction loss and increasing discharging performance of dielectrics at high temperatures.

2. Results and discussion

2.1 Preparation and structural characterization

Poly(chlorotrifluoroethylene-*co*-vinylidene fluoride) (Honeywell Aclar® VK grade with 2.5 mol% VDF, abbreviated as **VK**), a semi-crystalline thermoplastic polymer with a melting temperature (T_m) of ~220 °C and a T_g of ~100 °C, was chosen in this study. Different from poly(tetrafluoroethylene) (PTFE) which is notoriously difficult to process, **VK** is moldable by various techniques such as injection, extrusion and compression molding.[35] **VK** offers a unique combination of physical and mechanical properties, including non-flammability, high optical transparency, excellent chemical resistance, and near zero moisture absorption, and has attracted much interest for its commercial applications in medical and pharmaceutical packaging, but received almost no attention as a dielectric material. Our measurements show that **VK** exhibits outstanding room-temperature capacitive performance, which is comparable to BOPP (ESI Fig. S1 †). For example, the respective U_e and η of **VK** are 3.39 J cm^{-3} and 94.2% at 500 MV m^{-1}, and 4.83 J cm^{-3} and 90.9% at 600 MV m^{-1} measured at 25 °C. Comparatively, BOPP has an U_e of 2.41 J cm^{-3} and a η of 97.5% at 500 MV m^{-1}. However, the capacitive performance of **VK** drops rapidly with the increase of temperature (ESI Fig. S2 †), the typical characteristic of the current dielectric polymers. For example, at an applied field of 300 MV m^{-1}, U_e and η decrease from 1.04 J cm^{-3} and 60.7% at 100 °C to 0.57 J cm^{-3} and 37.9% at 150 °C, respectively.

The crosslinked **VK** (abbreviated as **XL-VK**) was prepared by melt-processing of the mixture of **VK**, dicumyl peroxide (DCP) as the initiator and 5 wt% triallyl isocyanurate (TAIC) as the co-agent. DCP decomposes to peroxide radicals, which abstract chlorine atoms from the polymer chain, leading to macromolecular radicals that are then reacted with TAIC to form a crosslinked network (Fig. 1 and ESI Figs. S3 †). Compared to other co-agents, such as ethylene glycol dimethacrylate, triallyl phosphate, triallylcyanurate, and 2,4,6-triallyloxy-1,2,5-triazine, TAIC is found to exhibit the lowest compression set and has been efficiently used in the formation of peroxide-induced crosslinked fluoropolymers.[17,36] The initiator concentration was deliberately varied from 2, 3 to 4 wt% in the preparation of the network, yielding the resultant film samples labelled as **XL-VK-1**, **-2** and **-3**, respectively. The cross-sectional scanning electron microscopic (SEM) image of XL-VK-2 is presented in ESI S4a†. The crosslinking reaction is confirmed by Fourier transform infrared (FTIR) spectroscopy (ESI Fig. S5 †) and X-ray photoelectron spectroscopy (XPS) (ESI Fig. S6 †). The impact of crosslinking on the crystallization behaviour was evaluated using differential scanning calorimetry (DSC) (ESI Fig. S7 †) and X-ray diffraction (XRD) (ESI Fig. S8 †). As expected, crosslinking decreases T_m, crystallinity (X_{XRD}) and crystallite size corresponding to the (101) plane, *i.e.* from 215 °C, 77.9% and 42.5 nm of **VK** to 198 °C, 70.4% and 35.2 nm of **XL-VK-1**, 196 °C, 66.9% and 33.6 nm of **XL-VK-2**, and 193 °C, 62.8% and 30 nm of **XL-VK-3**, respectively (ESI Table S1 †). It is known that an ordered crystalline phase is more conductive than an amorphous phase.[4] Therefore, the decrease in crystallinity is desirable as it would contribute to the reduced electrical conductivity across the polymers.

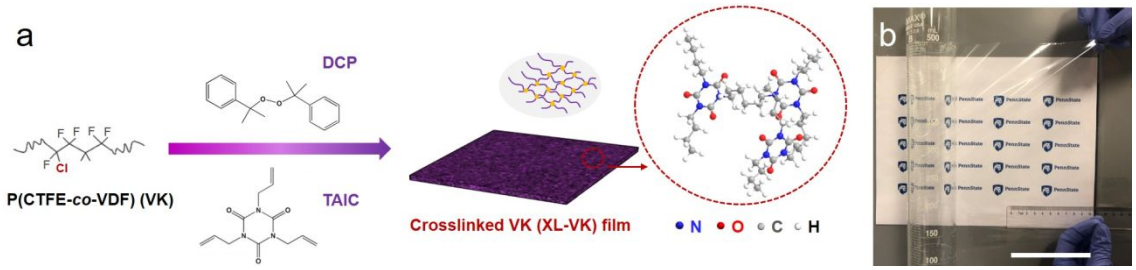

Fig. 1 Material preparation. (a) Schematic of the preparation of **XL-VK** films. (b) Photograph of a 12-μm-thick **XL-VK-2** film wrapped on a 500 mL graduated cylinder (Scale bar: 10 cm).

2.2 Dielectric properties and capacitive performance

Weak-field dielectric properties of the polymers have been characterized as a function of frequency and temperature (Fig. 2a and ESI Fig. S9†). As shown in Fig. 2a, the real part of permittivity (K) at 1 kHz increases from 2.88 of **VK** to 3.23 of **XL-VK-1**, 3.19 of **XL-VK-2** and 3.11 of **XL-VK-3**. The improved K in **XL-VK** can be attributed to their smaller crystallite sizes that are more easily aligned under the field. A high degree of crosslinking yields a dense network that would restrict the mobility of dipoles under the applied field, and consequently, a reduced K as shown in the decline trend from **XL-VK-1** to **-2** and **-3**. Meanwhile, the crosslinked polymers exhibit lower loss tangent (tanδ) than pristine **VK**, e.g. 0.0252 of **XL-VK-2** *vs*. 0.0284 of **VK** at 1 kHz. The slightly increased tanδ of **XL-VK-3** is owing to the presence of a high content of the polar groups from TAIC in the sample. The dielectric spectra of the polymers are recorded at varied

temperatures (ESI Fig. S10†), which is described well by the Arrhenius equation. As shown in Fig. 2b, the activation energy (E_a) of the *γ* relaxation calculated from the Arrhenius equation increases in **XL-VK**, *e.g.*, 0.78 eV of **XL-VK-2** *vs.* 0.65 eV of **VK**, indicating that the network formation hampers chain relaxation.

We measured the breakdown strength of the polymers at varied temperatures. ESI Fig. S11 † and ESI Table S2 †compares the characteristic breakdown parameters of the pristine and crosslinked **VK** analysed by using a two-parameter Weibull distribution function:

$$P(E) = 1 - \exp\left(\frac{E}{E_b}\right)^{\beta} \quad (1)$$

where $P(E)$ is the probability of breakdown, E is the measured breakdown field, E_b is the Weibull breakdown strength which is associated with the field strength at a 63.2% probability of breakdown, β is the shape parameter evaluating the scatter of experimental data. Compared with the current high-temperature polymer based dielectrics, **XL-VK-2** exhibits the greatest E_b of 681 MV m^{-1} at room temperature (ESI Fig. S12 †). While the polymers show a typical decrease in E_b with temperature, **XL-VK** displays significantly improved E_b, especially at elevated temperatures, when compared with the pristine polymer (Fig. 2c). For instance, at 100 °C and 150 °C, **XL-VK-2** has a E_b of 604 and 494 MV m^{-1}, respectively, which represent an ~100% enhancement than **VK** (*i.e.* 301 and 251 MV m^{-1}) and are even greater than E_b of PI (i.e. 314 MV m^{-1} at 150 °C), PEI (i.e. 439 MV m^{-1} at 150 °C) and the high-temperature dielectric composite *c*-BCB/BNNSs (*i.e.* 421 MV m^{-1} at 150 °C)[17] and *c*-BCB/Al_2O_3 nanoplates (NPLs) (*i.e.* 489 MV m^{-1} at 150 °C)[24] (*c*-BCB: cross-linked divinyltetramethyldisiloxane bis(benzocyclobutene)) as compared in Fig. 2d. Additionally, a pronounced increase of the β values is found in the crosslinked polymer, *e.g.*, 15.94 of **XL-VK-2** vs. 5.51 of **VK** at 150 °C, denoting a narrower distribution of experimental results and increased dielectric reliability of the crosslinked films.

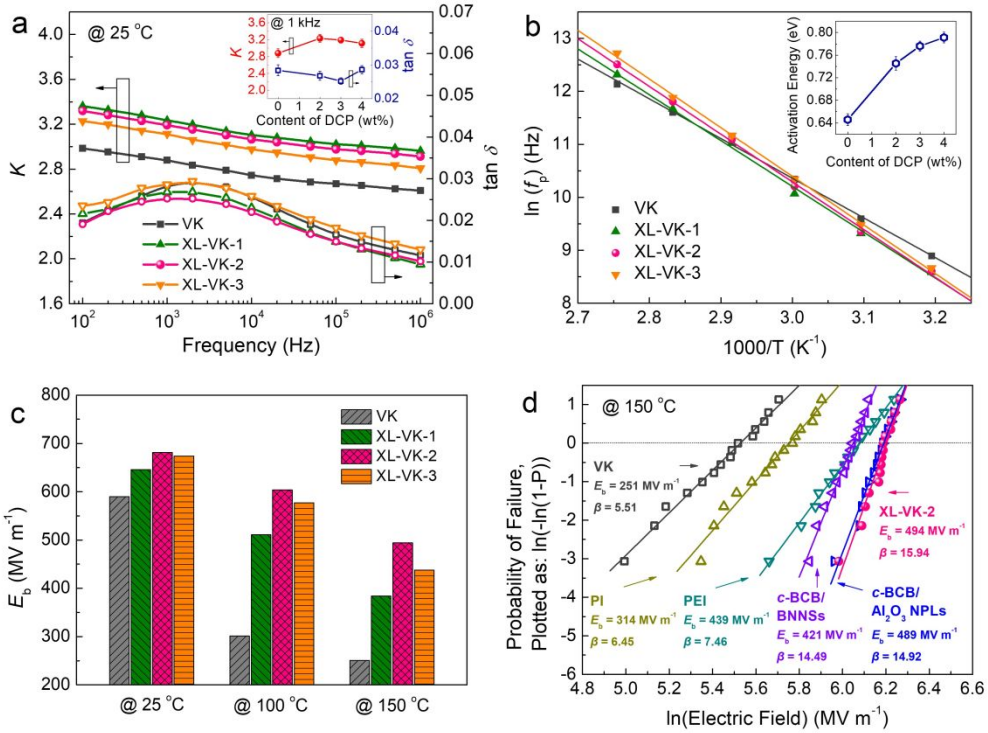

Fig. 2 Dielectric properties and breakdown strength. (a) Frequency-dependent dielectric spectra of **VK** and **XL-VK**. (b) Arrhenius plots of peak frequency from the imaginary part of permittivity spectra of **VK** and **XL-VK**. The inset is the activation energy of the *γ* relaxation as a function of DCP content. (c) Weibull Breakdown Strength (E_b) of **VK** and **XL-VK** measured at 25 °C, 100 °C and 150 °C, respectively. (d) Weibull statistic of dielectric breakdown strength of **VK**, **XL-VK-2**, PI, PEI and the *c*-BCB-based nanocomposites at 150 °C. Error bars in (a) and (b) represent standard deviations obtained from at least three measurements using different samples.

Slimmer electric displacement–electric field (*D*–*E*) loops with lower remnant polarization of **XL-VK** are evident in the typical loops displayed in ESI Fig. S13†, signifying its lower high-field dielectric loss relative to that of **VK**. As summarized in ESI Fig. S14†, the crosslinked polymers exhibit substantially enhanced high-temperature U_e and η in comparison with the neat polymer. More impressively, as shown in Figs. 3a-b, **XL-VK-2** delivers an U_e of 4.72 J cm^{-3} with a η of ~ 90% at 550 MV m^{-1} and 100 °C, and an U_e of 2.67 J cm^{-3} with a η of > 90% at 400 MV m^{-1} and 150 °C, which exceeds the crosslinked *c*-BCB and epoxy resin (ESI Fig. S15 †)[17,31,37], high-temperature dielectric polymers including PI, FPE, PEI, SO_2-PPO and SO_2-PIM[26,27], and polymer nanocomposites including PI/barium titanate nanofiber (BTNF), ternary PEI/barium titanate nanoparticle (BTNP)/BNNS, sandwich-structured *c*-BCB/BTNP/BNNS, and *c*-BCB/BNNS and the newly developed composite *c*-BCB/Al_2O_3 NPL[17,18,24,28,38–40] as compared in Fig. 3c. To the best of the our knowledge, the maximum U_e of 4.33 J cm^{-3} with a η of 70% at 526 MV m^{-1} is the highest U_e reported so far in dielectric polymers and polymer composites at 150 °C. Impressively, at an applied field of 200 MV m^{-1}, which is the operation condition of film capacitors in electric vehicles, **XL-VK-2**

exhibits outstanding η >97.7% over a wide temperature range of 25-150 °C (Fig. 3d). High η suggests much reduced Joule heating generated from the dielectric films, which would enable efficient operation of film capacitors with great reliability. The excellent η achieved from **XL-VK-2** at 150 °C would allow the elimination of the secondary cooling system currently applied onto the power inverter of electric vehicles, and consequently, result in a simplified integrated power system and greatly enhanced volumetric and energy efficiencies. On the other hand, it is found that the simple addition of TAIC into **VK** leads to deteriorated η and E_b at both room temperature and 150 °C (ESI Fig. S16 †), which further confirms the critical role of crosslinking in the capacitive performance.

As shown in Fig. 3e, at 200 MV m^{-1}, **XL-VK-2** possesses the highest K of 3.62 measured at 1 kHz and 150 °C relative to other high-temperature dielectric polymers and even the nanocomposites containing γ-Al_2O_3 fillers with a K of 9-10,[24] and thus yields the largest U_e of 0.67 J cm^{-3}, which is > 100% higher than U_e of BOPP operating at 100 °C.[40] It is estimated that a 100% increase in U_e corresponds to more than 17% reduction in weight and size of capacitors which occupy ~23% of weight and 35-40% of volume of the power inverter in electric vehicles.[19,21] In addition, it is found that **XL-VK-2** discharges a highly stable power density with respect to the operating temperature ranging from 25 to 150 °C, while a steadily decline in power density appears in BOPP with the increase of temperature (Fig. 3f and ESI Fig. S17†). Moreover, **VK-XL-2** shows no change in the film size under 150 °C for 24 h (ESI Fig. S4b-c†) and no sign of degradation in U_e and η (ESI Fig. S18 †) over 50,000 charge-discharge cycles operating at 200 MV m^{-1} and 150 °C.

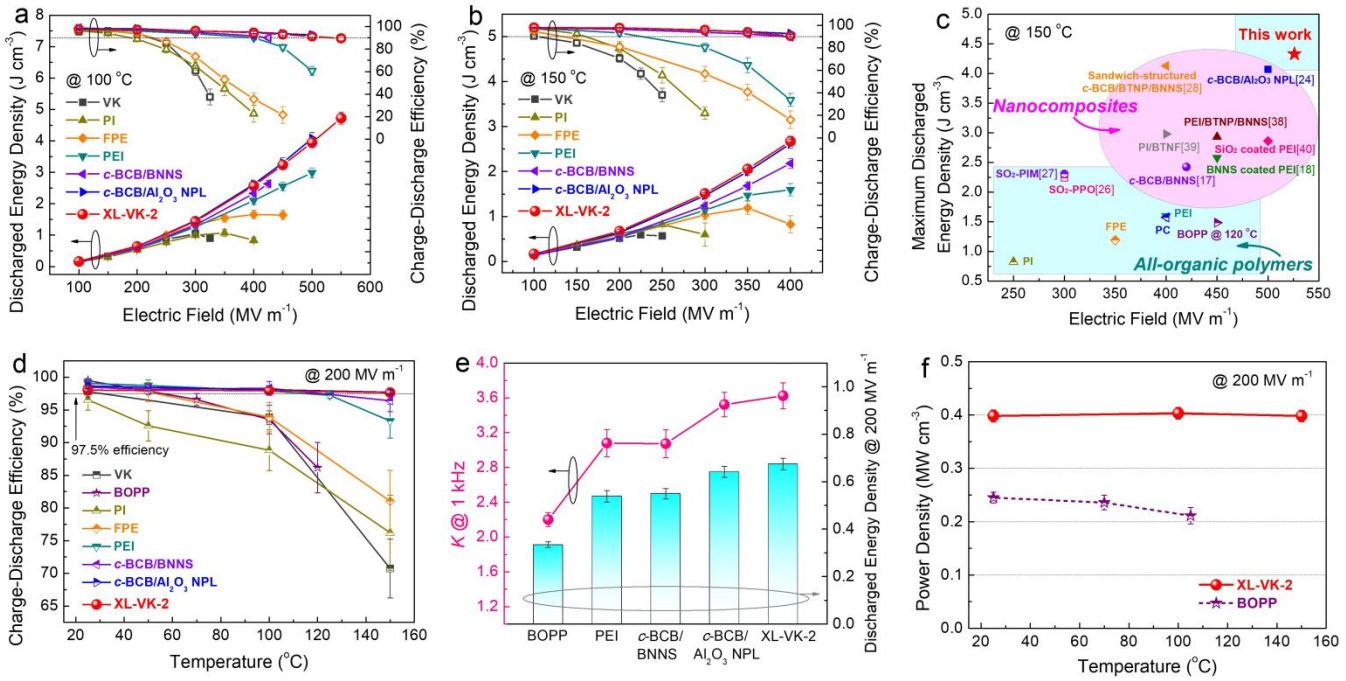

Fig. 3 Capacitive performance. Discharged energy density and charge-discharge efficiency of **VK**, **XL-VK** and high-temperature dielectrics at (a) 100 °C and (b) 150 °C, respectively. (c) Comparison of the discharged energy density of high-temperature dielectric polymers and polymer composites at 150 °C. (d) Charge-discharge efficiency of the dielectrics as a function of temperature measured at 200 MV m^{-1}. (e) Comparison of K at 1 kHz and the discharged energy density at 200 MV m^{-1} of high-temperature dielectrics at 150 °C and BOPP at 100 °C and. (f) Power density of BOPP and **XL-VK-2** as a function of temperature measured at 200 MV m^{-1}. Error bars in (a, b, d-f) represent standard deviations obtained from at least three measurements using different samples.

2.3 Electrical conduction and charge trapping

It is recognized that electrical conduction is the major high-field loss mechanism of dielectrics, which is responsible for substantially reduced U_e and η of dielectric materials when operating at elevated temperatures and high electric fields.[4,19,20] As shown in Fig. 4a and ESI Fig. S19†, the current density (J) is reduced by more than two orders of magnitude with crosslinking of **VK**, *e.g.*, from 7.81 × 10^{-10} and 6.99 × 10^{-7} A cm^{-2} of **VK** to 3.28 × 10^{-11} and 1.14 × 10^{-8} A cm^{-2} of **XL-VK-2** measured at 100 °C and 150 °C, respectively, at an applied field of 100 MV m^{-1}. More interestingly, it is found that the increase of J with the applied field is much less pronounced in **XL-VK-2** than those of the current dielectric polymers and polymer composites. At 150 °C, the ratio of J at 400 MV m^{-1} *vs.* J at 50 MV m^{-1} is 236 of **XL-VK-2**, whereas the corresponding values are 2060 of PI, 1340 of FPE, 318 of *c*-BCB/BNNSs and 251 of *c*-BCB/Al_2O_3 NPLs (ESI Fig. S20†). This comparison manifests the effectiveness of the crosslinked structures in hindering field-dependent electrical conduction at high temperatures. According to the hopping conduction model, J is given as,[5,24]

$$J(E,T) = 2ne\lambda * \exp\left(-\frac{W_a}{K_B T}\right) * \sinh\left(\frac{\lambda eE}{2K_B T}\right) \quad (2)$$

where n is the carrier concentration, λ is the hopping distance, v is the attempt-to-escape frequency, W_a is the activation energy in eV, e is the charge of the carriers, m is the mass of the free electron. The equation (2) can be simplified as

$$J(E) = A * \sinh(BE) \quad (3)$$

where *A* and *B* are two lumped parameters. As shown in Fig. 4b, the experimental *J* data fit well with the equation (3) with the quality of fitting, R^2, ranging from 0.983 to 0.997, indicating that hopping is the major conduction mechanism in **VK** and **XL-VK** at high temperatures and high fields. The hopping distance calculated by fitting the *J*-*E* data to the hopping conduction equation decreases markedly from 1.88 nm of **VK** to 1.36 nm of **XL-VK-1**, 1.23 nm of **XL-VK-3**, and 0.92 nm of **XL-VK-2**. As a shorter hopping distance corresponds to a deeper trap depth, the highest trap depth accounts for the largest drop in *J* and the most significant increases in U_e and η observed in **XL-VK-2**. The presence of a higher content of the functional groups such as carbonyls in **XL-VK-3**, which act as shallower hopping sites, is responsible for increased *J* and reduced E_b.

The measurement of thermally stimulated depolarization currents (TSDC) has been carried out to assess the traps in the polymers. As shown in Fig. 4c, the peaks centered around -60 °C and 10 °C are related to the γ_c and γ_a relaxation associated with local motions in the crystalline and amorphous phases, respectively.[41] The β relaxation, which is ascribed to the glass transition of the polymer, increases from ~95 °C of **VK** to ~105 °C of **XL-VK-2** as a result of restricted chain mobility in the crosslinked structure.[41] Upon crosslinking, a high temperature peak centered at 155-160 °C, known as the α relaxation, appears in **XL-VK**. The consistent increase of the intensity of the α relaxation with increasing the initiator concentration from **XL-VK-1**, to **-2** and **-3** is apparently attributed to the increase of trap density. Since the depolarization current originates from electrons and holes, the trap energy level A_{TSDC} and the trapped charge quantity Q_{TSDC} can be obtained from TSDC curves according to the half-width method given by[42]

$$A_{\mathrm{TSDC}} = \frac{2.47 K_{\mathrm{B}} T_{\mathrm{p}}^2}{\Delta T} \quad (4)$$

where K_B is the Boltzmann constant, T_p is the temperature corresponding to the peak current and ΔT is the peak with at half height.

$$Q_{\mathrm{TSDC}} = (\frac{60}{\upsilon}) \int_{T_1}^{T_0} I(T) dT \quad (5)$$

where υ is the heating rate, T_0 and T_1 represent the starting temperature and ending temperature of peaks, respectively and $I(T)$ describes the depolarization current curve. As summarized in ESI Table S3 †, A_{TSDC} increases from 0.57 eV of **VK** and is maximized at 1.03 eV of **XL-VK-2**, indicative of the formation of the deepest trap level. This correlates well with the dielectric and capacitive results, in which the smallest *J*, lowest loss, and the highest U_e and η are found in **XL-VK-2**. Interestingly, it is found that the variation of E_b follows the trend of A_{TSDC} (ESI Fig. S21 †). The steady increase of Q_{TSDC} with crosslinking from **XL-VK-1** to **-2** and **-3** is ascribed to the presence of high contents of the double bonds and carbonyls from the initiator and co-agent that could act as shallow traps.

The embedded charges and traps in dielectric films have been further investigated by using the pulsed electroacoustic (PEA) measurement. ESI Fig. S22† shows the charge decay profiles at varied temperatures. ESI Fig. S23 † shows the room-temperature charge parameters as a function of decay time. It is found that at 25 °C, the average charge density $q(t)$ at moment *t* inside the sample decreases from 0.51 to 0.44 C m^{-3} in **VK** and from 0.31 to 0.26 C m^{-3} in **XL-VK-2** as time varies from 10 to 3600 s. At 80 °C, the corresponding $q(t)$ decays from 1.08 to 0.84 C m^{-3} in **VK** and from 2.54 to 2.34 C m^{-3} in **XL-VK-2** (Fig. 4d). Apparently, these results reaffirm the existence of more traps in **XL-VK-2**, which give rise to a lower $q(t)$ at 25 °C but a higher $q(t)$ with increasing temperature because the trapped charges are thermally activated. Moreover, at 25 °C, the charges released during the depolarization process are found to be trapped in a wider range of trap depths from 0.86 to 1.10 eV in **XL-VK-2** than that in **VK**, *i.e.* between 0.90 and 1.04 eV. This is consistent with the TSDC results, which is due to the presence of both shallow and deep traps in **XL-VK-2** introduced by the crosslinking reaction. The existence of traps with high energy barriers is again evident in **XL-VK** at elevated temperatures, which dictates the high-field electrical conduction behaviour of materials. At 80 °C, the trap depth in **XL-VK-2** is between 1.15 and 1.25 eV, which is much deeper than that of **VK**, *i.e.* 1.11 to 1.22 eV (Fig. 4e). Consequently, as shown in Fig. 4f, the reduction in the apparent mobility $\mu(t)$ is significant, *i.e.* from 7.60 × 10^{-14} to 1.60 × 10^{-15} m^2 V^{-1} s^{-1} of **XL-VK-2** and from 7.58 × 10^{-15} to 2.15 × 10^{-16} m^2 V^{-1} s^{-1} of **VK** with a decay time of 3600 s.

Journal Name

ARTICLE

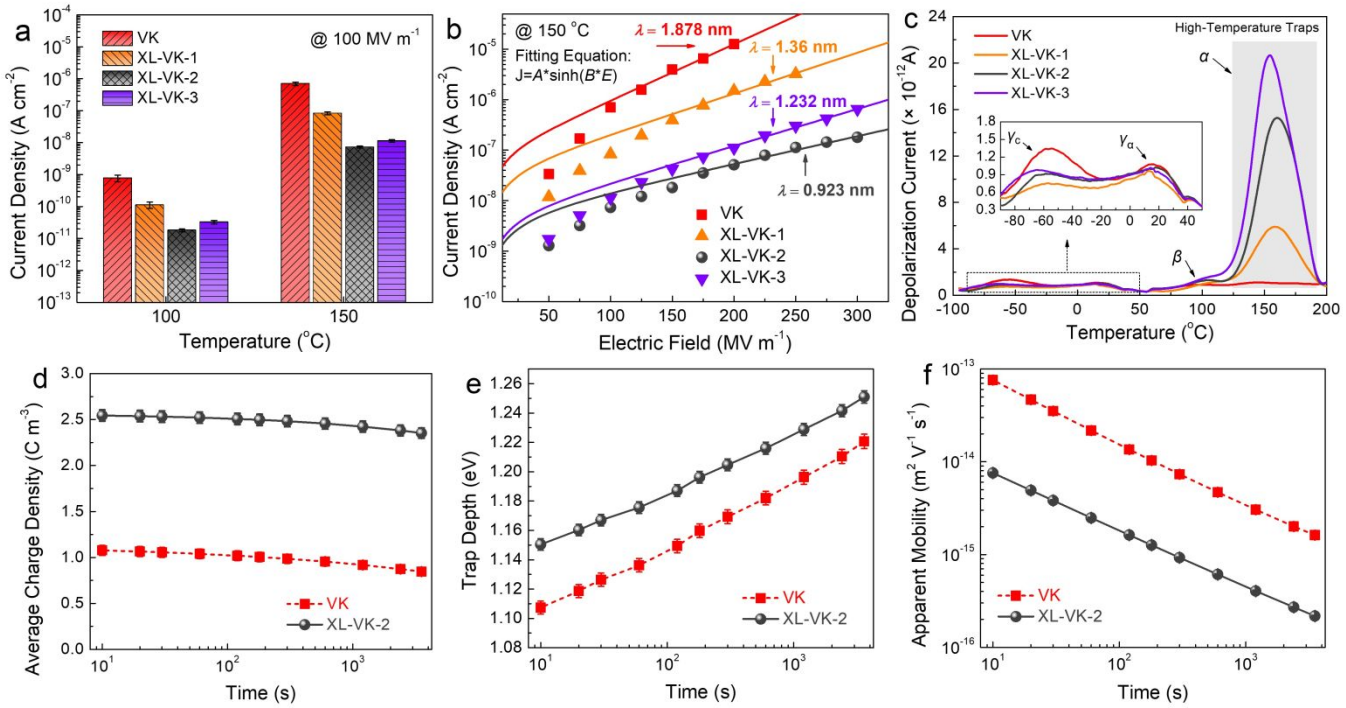

Fig. 4 Electrical conduction and trap-related parameters. (a) Conduction current density of **VK** and **XL-VK** measured at an applied field of 100 MV m^{-1} at 100 °C and 150 °C, respectively. (b) Conduction current density of **VK** and **XL-VK** as a function of electric field at 150 °C. Solid curves represent fit to hyperbolic sine. (c) TSDC curves of **VK** and **XL-VK**. The inset is the enlarged part of temperature range from -90-50 °C. (d) Average charge density, (e) Trap depth, and (f) Apparent mobility of **VK** and **XL-VK-2** as a function of decay time at 80 °C, respectively. Error bars in (a) and (d-f) represent standard deviations obtained from at least three measurements using different samples.

3. Conclusions

We have developed all-polymer high-temperature capacitive materials based on the crosslinked fluoropolymers and demonstrated excellent high-temperature capacitive performance, which outperforms the current dielectric polymers. Moreover, the crosslinked polymers exhibit excellent capacitive stability over 50,000 charge-discharge cycles at 150 °C and discharge a stable power density over a wide temperature range. In particular, the selection of moldable polymers would facilitate scalable preparation that is compatible with the current fabrication techniques used for polymer dielectrics. On the other hand, although the use of the inorganic fillers is shown to be beneficial in improving high-temperature discharging performance of polymers, the scalability of the resulting dielectric polymer composites remains elusive. We established through comprehensive measurements that the molecular trapping centers created by the crosslinked structures can effectively limit charge transport and reduce conduction loss at elevated temperatures and high applied electric fields. These features offer new opportunities for designing scalable organic dielectric materials capable of operating at extreme conditions. We envision that the structure tunability and designability of polymers and crosslinking chemistry will allow the further development of novel high-temperature energy materials for compact, lightweight and robust energy storage systems.

Experimental section

Preparation of VK and XL-VK films: VK polymer were given by Honeywell. Dicumyl peroxide (DCP) and triallyl isocyanurate (TAIC) were purchased from Sigma Aldrich and used without further purification. 2/5 wt%, 3/5 wt% and 4/5 wt% DCP/TAIC with respect to **VK** were added during freezer milling for **XL-VK-1**, **-2** and **-3** samples. **XL-VK** films were melt-prepared by heating at 255 °C with increasing the pressure by 500 psi every 5 min up to 7000 psi and then stretching at 180 °C to a draw ratio of ~2. The prepared samples were finally treated at 200 °C under vacuum for 12 hr to remove residual TAIC and crosslinking byproducts. For comparison, pristine **VK** films without the addition of DCP and TAIC and the VK films with

5 wt% TAIC were prepared using the same procedure. Considering the spatial resolution in PEA instruments, the film samples with the thickness of 180~200 μm were used in space charge measurements. The films for structural characterization and the other electrical measurements varies in thickness from 10~20 μm. For all the electrical measurements, both sides of the films were sputter coated with gold electrodes with a thickness of 60 nm and a diameter of 0.26 mm for dielectric breakdown and *D*–*E* loop measurements, 0.65 mm for dielectric spectroscopy, discharging, conduction current and TSDC measurements, and 2.4 cm for space charge measurements.

Structural characterization: SEM was performed by using a FEI Nova NanoSEM 630 field emission electron microscope. The embrittlement section of film sample was obtained in liquid nitrogen, and vacuum sputterred with a thin gold layer prior to observation. FTIR spectra were obtained in an attenuated total reflectance (ATR) mode equipped with a ZnSe crystal as a contact to the samples on a Bruker Vertex 70 spectrometer at room temperature. XPS (K-Alpha Plus, Thermo Fisher) was adopted to analyze the chemical compositions of the films. DSC curves were acquired using a TA instrument model Q100 with a heating and cooling rate of 10 °C min^{-1} under nitrogen atmosphere. XRD analysis was studied using a PANalytical Xpert Pro MPD θ–θ diffractometer. The radiation source was a Cu Kα source with a wavelength of 1.54 Å.

Dielectric spectroscopy and breakdown measurements: Dielectric spectra were collected over a board frequency range from 10^2 Hz to 10^6 Hz and a temperature range from -50 °C to 200 °C by a Hewlett Packard 4284 LCR meter in conjunction with a Delta Design 2300 oven equipped with a liquid nitrogen cooling system. The activation energy of the Debye-like *γ* relaxation is determined from the temperature dependence of corresponding peak frequency from the imaginary part of permittivity spectra, which typically linear fits an Arrhenius relationship given as,[24,41]

$$f_{\mathrm{p}}(T) = f_0 * \exp\left(-\frac{E_{\mathrm{a}}}{K_{\mathrm{B}}T}\right) \quad (6)$$

where f_{p} is the frequency corresponding to the relaxation peak, f_0 is a constant, E_{a} is the activation energy of relaxation process, T is the temperature in Kelvins, and K_{B} is the Boltzmann constant. Dielectric breakdown strength measurements were performed in high-temperature insulation fluid at varied temperatures, using a TREK P0621P instrument and setup applying a DC ramp voltage of 500 V s^{-1} until breakdown. The temperature was controlled utilizing a digital hot plate equipped with a thermal couple. The breakdown strength was evaluated by performing two-parameter Weibull distribution analysis on ≥ 15 samples.

Electric displacement–electric field (*D*–*E*) loop and discharge measurements: *D*–*E* loops were collected using a modified Sawyer–Tower circuit with a Trek Model 30/20 ± 30 kV High Voltage amplifier system, using a triangular unipolar wave with a frequency of 10 Hz. The capacitive performance of dielectric materials is evaluated from the *D*–*E* loops as shown in ESI Fig. S10†. Fast discharge tests were carried out through a capacitor discharge system with a high-voltage metal oxide semiconductor field effect transistor (MOSFET) switch (Behlke HTS81). The typical charging time was ~10 μs and the resistance of the load resistor was selected as 6.5 kΩ. All the *D*–*E* loop and fast discharging were performed in high-temperature insulation fluid. The temperature was controlled utilizing a digital hot plate equipped with a thermal couple.

Electrical conduction and TSDC measurements: Conduction currents and TSDC spectra were obtained using a Hewlett Packard 4140B pA meter with Kepco BOP 1000M amplifier as a High Voltage source in conjunction with a Delta Design 2300 oven equipped with a liquid nitrogen cooling system. The conduction current density (*J*) was measured at various applied fields and temperatures.

The samples for TSDC measurements were annealed at 150 °C for 10 min before poled at 150 °C for another 10 min under an applied field of 50 MV m^{-1}, and then rapidly cooled to -100 °C while maintaining electric field. Samples were then short-circuited and heated at a rate of 3 °C min^{-1} with the depolarization currents recorded up to 200 °C.

Space charge measurements: Space charge parameters were measured by using a PEA system in conjunction with a temperature control equipment containing high-temperature insulation fluid. After polarizing at 70 MV m^{-1} for two hours, the charge dissipation behaviors inside the samples during the depolarization process were measured for one hour at 25 °C and 80 °C, respectively. The average charge density, the trap depth and the apparent mobility of samples were then calculated based on the space charge measurement results.[43]

$$\boldsymbol{q(t)} = \frac{\mathbf{1}}{\boldsymbol{d}}\int_{\mathbf{0}}^{\boldsymbol{d}} |\boldsymbol{q_p(x,t)}|\,\mathbf{d}\boldsymbol{x} \quad (7)$$

where d is the thickness of the sample, $q_{\mathrm{p}}(x,t)$ is the charge density at position x and moment t. Based on the variation curve of average charge density $q(t)$ with time t during the depolarization process, the trap depth $\Delta U(t)$ can be fitted from the following model.

$$q(t) = \sum_{i=2}^{m} n_i(0)\exp\left[-\nu\exp\left(\frac{\Delta U}{K_{\mathrm{B}}T}\right) * t\right] \quad (8)$$

where $n_i(0)$ is the density of charges trapped in the i^{th} level at t = 0 s, $\nu = K_{\mathrm{B}}T/h$ is the attempt frequency, in which k is the Boltzmann constant, T is temperature in Kelvin and h is the Planck constant. The corresponding trap-controlled apparent mobility $\mu(t)$ inside the samples can be calculated from

$$\mu(t) = \frac{2}{q^2(t)}\frac{\mathrm{d}q(t)}{\mathrm{d}t} \quad (9)$$

Conflicts of interest

There are no conflicts to declare.

Acknowledgements

The authors acknowledge the support from the US Office of Naval Research under grant number N00014-11-1-0342. H.L. thanks Prof. Z.R. Peng and S.Y. Zhang at Xi'an Jiaotong University for their assistance with PEA analysis, and Prof. Y. Liu and Dr. X.L. Li at Lawrence Berkeley National Laboratory for their assistance with XPS analysis.

Notes and references

1 R. W. Johnson, J. L. Evans, P. Jacobsen, Thompson, J. R. and M. Christopher, *IEEE Trans. Electron. Packag. Manuf.*, 2004, **27**, 164.
2 J. Watson and G. Castro, *J. Mater. Sci.- Mater. El.*, 2015, **26**, 9226.

3 J. Zhang, J. Zhao, L. Yue, Q. Wang, J. Chai, Z. Liu, X. Zhou, H. Li, Y. Guo, G. Cui and L. Chen, *Adv. Energy Mater*. 2015, **5**, 1501082.
4 M. Ieda, *IEEE Trans. Electr. Insul.*, 1984, **3**, 162.
5 J. S. Ho and T. R. Jow, *IEEE Trans. Dielectr. Electr. Insul.*, 2012, **19**, 990.
6 Z. M. Dang, J. K. Yuan, J. W. Zha, T. Zhou, S. T. Li and G. H. Hu, *Prog. Mater. Sci.*, 2012, **57**, 660.
7 X. Huang and P. Jiang, *Adv. Mater.*, 2015, **27**, 546.
8 H. Li, F. Liu, B. Fan, D. Ai, Z. Peng and Q. Wang, *Small Methods*, 2018, **2**, 1700399.
9 Z. M. Dang, J. K. Yuan, S. H. Yao and R. J. Liao, *Adv. Mater.*,2013, **25**, 6334.
10 B. Chu, X. Zhou, K. Ren, B. Neese, M. Lin, Q. Wang, F. Bauer and Q. M. Zhang, *Science*, 2006, **313**, 334.
11 S. Luo, J. Yu, S. Yu, R. Sun, L. Cao, W. H. Liao and C. P. Wong, *Adv. Energy Mater.*, 2019, **9**, 1803204.
12 Y. Wang, L. Wang, Q. Yuan, J. Chen, Y. Niu, X. Xu, Y. Cheng, B. Yao, Q. Wang and H. Wang, *Nano Energy*, 2018, **44**, 364.
13 Q. Li, G. Zhang, F. Liu, K. Han, M. R. Gadinski, C. Xiong and Q. Wang, *Energy Environ. Sci.*, 2015, **8**, 922.
14 Z. Pan, J. Zhai and B. Shen, *J. Mater. Chem. A*, 2017, **5**, 15217.
15 S. Luo, Y. Shen, S. Yu, Y. Wan, W. H. Liao, R. Sun and C. P. Wong, *Energy Environ. Sci.*, 2017, **10**, 137.
16 L. Xie, X. Huang, C. Wu and P. Jiang, *J. Mater. Chem.*, 2011, **21**, 5897.
17 Q. Li, L. Chen, M. R. Gadinski, S. Zhang, G. Zhang, H. U. Li, E. Iagodkine, A. Haque, L. Q. Chen, T. Jackson and Q. Wang, *Nature*, 2015, **523**, 576.
18 A. Azizi, M. R. Gadinski, Q. Li, M. A. AlSaud, J. Wang, Y. Wang, B. Wang, F. Liu, L. Q. Chen, N. Alem and Q. Wang, *Adv. Mater.*, 2017, **29**, 1701864.
19 Q. Li, F. Z. Yao, Y. Liu, G. Z. Zhang, H. Wang and Q. Wang, *Annu. Rev. Mater. Res.*, 2018, **48**, 219.
20 J. S. Ho and S. G. Greenbaum, *ACS Appl. Mater. Interfaces*, 2018, **10**, 29189.
21 K. Bennion and M. Thornton, Presented at SAE World Cong., Detroit, MI, SAE Tech. Pap., 2010, 01-0836.
22 P. G. Neudeck, R. S. kojie, and L. Y. Chen, *Proc. IEEE*, 2002, **90**, 1065.
23 Z. H. Shen, J. J. Wang, J. Y. Jiang, Y. H. Lin, C. W. Nan, L. Q. Chen and Y. Shen, *Adv. Energy Mater.*, 2018, **8**, 1800509.
24 H. Li, D. Ai, L. Ren, B. Yao, Z. Han, Z. Shen, J. Wang, L. Q. Chen and Q. Wang, *Adv. Mater.*, 2019, **31**, 1900875.
25 Z. H. Shen, J. J. Wang, J. Y. Jiang, S. H. Huang, Y. H. Lin, C. W. Nan, L. Q. Chen and Y. Shen, *Nat. Commun.*, 2019, **10**, 1843.
26 Z. Zhang, D. H. Wang, M. H. Litt, L. S. Tan and L. Zhu, *Angew. Chem. Int. Ed.*, 2018, **130**, 1544.
27 Z. Zhang, J. Zheng, K. Premasiri, M. H. Kwok, Q. Li, R. Li, S. Zhang, M. H. Litt, X. P. A. Gao and L. Zhu, *Mater. Horiz.*, 2020. DOI: 10.1039/C9MH01261C
28 Q. Li, F. Liu, T. Yang, M. R. Gadinski, G. Zhang, L. Q. Chen and Q. Wang, *Proc. Natl. Acad. Sci. U. S. A.*, 2016, **113**, 9995.
29 T. L. Hanley, R. P. Burford, R. J. Fleming and K. W. Barber, *IEEE Electr. Insul. Mag.*, 2003, **19**, 13.
30 Q. Zhou, J. Ma, S. Dong, X. Li, and G. Cui, *Adv. Mater.*, 2019, **31**, 1902029.
31 P. Khanchaitit, K. Han, M. R. Gadinski, Q. Li and Q. Wang, *Nat. Commun.*, 2013, **4**, 2845.
32 N. L. Meereboer, I. Terzić, P. van der Steeg, G. Portale and K. Loos, *J. Mater. Chem. A*, 2019, **7**, 2795.
33 X. Z. Chen, Z. W. Li, Z. X. Cheng, J. Z. Zhang, Q. D. Shen, H. X. Ge and H. T. Li, *Macromol. Rapid Commun.*, 2011, **32**, 94.
34 S. Tan, X. Hu, S. Ding, Z. Zhang, H. Li and L. Yang, *J. Mater. Chem. A*, 2013, **1**, 10353.
35 H. Teng, *Appl. Sci.*, 2012, **2**, 496.
36 A. Taguet, B. Ameduri and B. Boutevin, *Adv. Polym. Sci.* 2005, **184**, 127.
37 S. Chen, G. Meng, B. Kong, B. Xiao, Z. Wang, Z. Jing, Y. Gao, G. Wu, H. Wang and Y. Cheng, *Chem. Eng. J.*, 2020, **387**, 123662.
38 H. Li, L. Ren, D. Ai, Z. Han, Y. Liu, B. Yao and Q. Wang, *InfoMat*, 2019. DOI: 10.1002/inf2.12043
39 P. Hu, W. Sun, M. Fan, J. Qian, J. Jiang, Z. Dan, Y. Lin, C. W. Nan, M. Li and Y. Shen, *Appl. Surf. Sci.*, 2018, **458**, 743.
40 Y. Zhou, Q. Li, B. Dang, Y. Yang, T. Shao, H. Li, J. Hu, R. Zeng, J. He and Q. Wang, *Adv. Mater.*, 2018, **30**, 1805672.
41 H. Shimizu and K. Nakayama, *Jpn. J. Appl. Phys.*, 1989, **28**, L1616.
42 C. Christodoulides, *J. Phys. D Appl. Phys.*, 1985, **18**, 1501.
43 G. Mazzanti, G. C. Montanari and J. M. Alison, *IEEE Trans. Dielec. Electr. Insul.*, 2003, **10**, 187.

Broader context

Polymers are the material of choice for capacitive energy storage materials in many power electronics, power conditioning, and pulsed power applications owing to their inherent advantages such as easy processability, high breakdown strength and graceful failure mechanism. However, current dielectric polymers are limited to relatively low working temperatures especially under the application of an electric field, which fails to meet the rising demand of electrical energy storage under the extreme conditions such as those in electric vehicles, aerospace systems and power grids. While promising elevated-temperature capacitive performance has been achieved in the polymers filled with inorganic fillers, the scalability of the resulting composites remains elusive as they are typically prepared by tedious, complex and time-consuming methods that are incompatible with the current melt-based processes used for polymer dielectrics. Herein we present a class of melt-processable all-polymer based high-temperature dielectric materials that can operate efficiently at high temperatures (e.g. 150 ^{o}C) and high electric fields, which exceeds the capacitive performance of the current dielectric polymers. The molecular trapping centers yielded from the crosslinked structures have been demonstrated to be effective in impeding electrical conduction at high fields and elevated temperatures. This result has significant impacts on the design of all-organic energy materials for extreme-condition applications. This work also provides new fundamental insights into the mechanisms that control electrical conduction in polymers at high temperatures under the applied electric fields.

Journal Name

ARTICLE

Table of contents entry

Superior high-temperature discharged energy densities in comparison to those of the current dielectric polymers have been demonstrated in the crosslinked fluoropolymers.